Research Article ISSN 2832-9384

Journal of Materials and Polymer Science

Role of D Electrons in Multifunctional Materials

Nabanita Dutta, S. K. Bandyopadhyay*, Subhasis Rana, Pintu Sen and A.K. Himanshu

Department of Basic Science and Humanities, Institute of Engineering and Management, University of Engineering and Management, Kolkata-700160, India.

***Corresponding author**

S. K. Bandyopadhyay,
Department of Basic Science and Humanities,
Institute of Engineering and Management,
University of Engineering and Management,
Kolkata-700160, India.

Submitted : 1 May 2025 ; Published : 11 Jul 2025

Citation: Dutta, N. et al. (2025). Role of d electrons in Multifunctional Materials. *J mate poly sci, 5*(2) :1-5.
DOI : https://doi.org/10.47485/2832-9384.1074

Abstract

Multifunctional materials are of today's quest. A class of multifunctional materials display simultaneous ordering in different dimensions like magnetism, polarization etc. They are more known as multiferroics. Quite a significant number of them are based on perovskite structures having a transition metal ion in the body centre. The electronic configuration of this central transition element play a key role in the behavior of those multiferroics. For example, those with d0 configuration display ferroelectricity while those with dn (where n is non zero) generally display magnetic behavior. The d0 configuration leads to distortion of metal-oxygen bond in these perovskites and breaking of special inversion symmetry causing a local dipole moment and ferroelectricity. Often this distortion in metal-oxygen bond is caused by lone pair of electrons non-transitional cations in the corners of the perovskite structure.BiFeO3 (BFO) is a shining example of this kind of distortion, where the central ion Fe(III) causes magnetism but Bi(III) ions in the corner cause the polarization leading to the multiferroicity in BFO displaying both ferroelectric and antiferromagntic ordering. The symmetry breaking manifests in different kinds of ordering. Moreover, the variable valency of the central transition metal ion with d electrons manifests in redox behavior in these materials leading to various uses. We have observed such various functions in the multiferroic BFO like ferroelectric, magnetic and specific capacitance as high as 450F/gm rendering these materials useful in green energy storage materials. Moreover these redox behavior of these transition metal ion also leads to antimicrobial behavior in BFO.

Introduction

Since the end of last century, a class of materials called multifunctionals are of quite interest. As the name suggests, they can render various functions displaying a wide range of properties which can be useful in different sectors. For example, simultaneous magnetic and ferroelectric properties are displayed by these materials. They are sometimes denoted as multiferroic properties the term feroic associated with ordering, magnetic, electric or elastic. One of the essential component of these multiferroic materials is a transition element with unoccupied d orbitals. Presence of these d electrons with different configurations gives rise to ferroelectric or magnetic properties. Moreover, due to various oxidation states with elements containing unoccupied d orbitals, these materials often exhibit high capacitance-supercapacitor, quite useful I the context of green storage energy cell.

We have chosen Bismuth Ferrite BiFeO3 (BFO) based on Perovskite structure ABO_3 with Fe(III) playing the role of central transition element B at base centre, nontransition element Bi(III) occupying the corner points and Oxide ions at the face centre positions. Fe(III)-Fe(II) acts as redox system and also Fe(III) plays magnetic role. Here, Bi(III) ions with lone pair 6s electrons cause a repulsion to the nearby Oxide ions causing a distortion in Bi-O bonds leading to a polarization and ferroelectricity in BFO.

In this context, it is quite interesting to study the capacitance of multifunctional materials like the multiferroic Bismuth ferrite (BFO) showing coexistence of ferroelectricity as well as antiferromagnetism with wide applications (Zhang et al., 2005). Lokhande et al. (2007) observed specific capacitance value of 81F/gm in BFO films. Attempts have been made to obtain BFO in 1-Dimensional nanostructure forms like nanowire, nanorod, etc. (Gao et al., 2006; Xie et al., 2008). The nanostructured forms can be expected to offer better efficiency owing to large surface area giving rise to a high value of specific capacitance, for example in α-$MnMoO_4$ nanorods (Purusothaman et al., 2012).

In this paper, we report the development of BFO in different nanostructured forms like nanoparticle developed by bottom up approach, nanorod by the wet chemical template assisted method and its capacitance studies by electrochemical means. We have evaluated specific capacitance both through cyclic voltammetry at different scanning rates and charge-discharge

studies. Also we have studied BFO nanoparticles developed by bottom up approach. Studies have been carried out with respect to magnetic, polarization and magneto capacitance to look into multiferroic behavior with magneto electric coupling.

Experimental

BFO Nanoparticles

Bismuth and ferric nitrate were employed as starting material with 2-methoxymethanol as solvent for developing BFO nanomaterial. In this case, use of capping agent was avoided. The prepared solution was kept under reflux condition at a temperature of 80^0C for 6 hours and dense sol obtained was filtered, dried and then sintered at a temperature of 450^0C for 4 hours. The sintered powder consisted of some impurity of Bi-rich phase and it was leached with 0.01M nitric acid to eliminate those impurity phases. The sintered material was characterized with respect to crystal structure by X-Ray Diffraction (XRD) using Bruker D8 Advance X-ray Diffractometer. The particle size was obtained through Transmission Electron Microscope (TEM) (Model: FEIT20 with applied voltage of 200KV). Magnetization studies were done with Quantum Design SQUID Magnetometer.

BFO Nanorod

Anodized Aluminium Oxide (AAO) templates of 60 µm thickness and 13 mm diameter with pore size distribution ranges from 20-100 nm were employed. 0.1M solutions of Bi(NO3)3 and $Fe(NO_3)_3$ were prepared with stoichiometric amounts of the nitrates using methoxymethanol as solvent with pH adjusted to 2-3. The filling of nanopores was achieved by the directional flow of the ions in the template adopting the controlled vacuum technique. The templates with pores containing solution were sintered for 3 hours at 7500C to get the required phase without unwanted grain growth. We attempted controlled etching process with 1M NaOH and the bundle of nanowires and nanorods emerged. Weights of BFO nanorods measured using a very sensitive microbalance (resolution of 1µgm) by subtracting the weights of respective AAO were in the range 80-100µg.

The nanowires and nanorods were examined by FEI Scanning Electron Microscope (SEM) with a resolution of 6nm aided by Energy Dispersive X-Ray (EDX) for compositional analysis. Transmission electron microscopy (TEM) was done by high resolution TEM (Model: FEI T20 with applied voltage of 200KV). Selective Area Electron Diffraction (SAED) was also undertaken to ascertain crystal structure of the nanorods.

Cyclic Voltammetry (CV) and galvanostatic charge-discharge were studied with AUTOLAB-30 potentiostat/galvanostat for both BFO on AAO and AAO blank templates being used as electrodes. The half etched templates used in SEM were employed for this purpose with the protrusion length of 1µm (as visible by SEM) over the template of thickness 60µm. Electrodes were prepared by connecting Cu lids with AAO/BFO templates through conducting silver paste. All the electrochemical experiments (i.e CV, Charge-discharge) were performed with two-electrode system having identical electrodes with respect to shape, size and made of same active electrode materials (i.e. Type-I symmetric supercapacitor) using an electrolyte containing 1M Na_2SO_4 in water. A platinum electrode and a saturated Ag/AgCl electrode were used as counter and reference electrodes respectively. All the CVs were measured between -0.6 to +0.6 V (i.e. operating window of 1.2V) with respect to reference electrode at different scan rates (5mV/s to 50mV/s). Constant currents ranging from 15 to 30 µAmp have been employed for charging/discharging the cell in the voltage range from -0.6 to +0.6 V.

Results and Discussions

BFO Nanoparticles

Fig. 1 displays XRD pattern for BFO Nanoparticle samples after leaching with HNO_3. Indexing of reflection planes of XRD pattern reveals the rhombohedrally distorted perovskite type cell with space group R3c free from any Bi or, Fe-rich phase. Grains fall in the range of approximately 50-60nm with as revealed from TEM in fig.2.

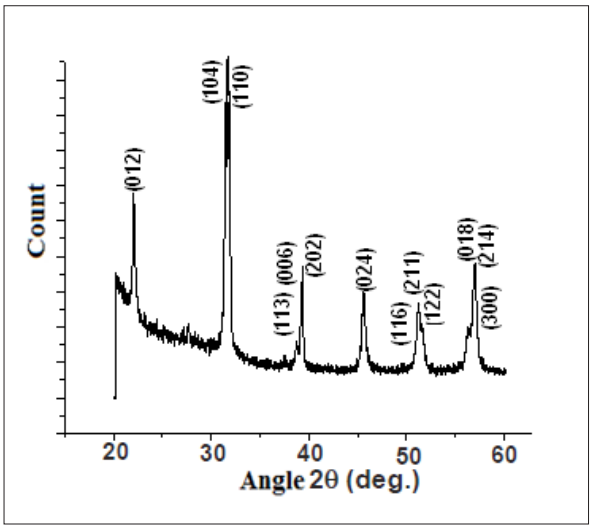

Figure 1: XRD pattern of BFO Nanoparticles. Characteristic peaks of BFO are present.

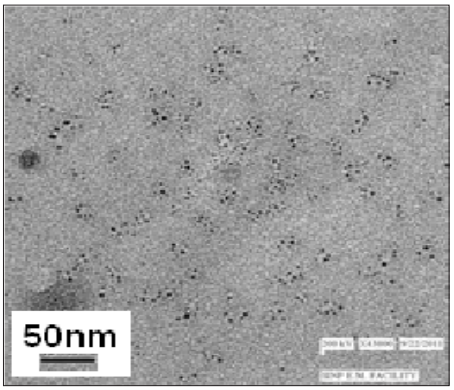

Figure 2: TEM micrography of BFO Nanoparticles. Particle size distribution from 5-50nm is noticed.

Fig. 3 displays zero field cooling (ZFC) and field cooling (FC) up to 5K using a field of 1000 Oe. M-H hysteresis loops were taken at 10K, 100K and 300K respectively and are depicted in Fig 4. It has shown ferromagnetic nature at 10K evident from

wide hysteresis loop with a remnant magnetization of ~3 emu/gm and a coercive field of ~700Oe. There is a sign of saturation at a field of ~2500 Oe at 10K.

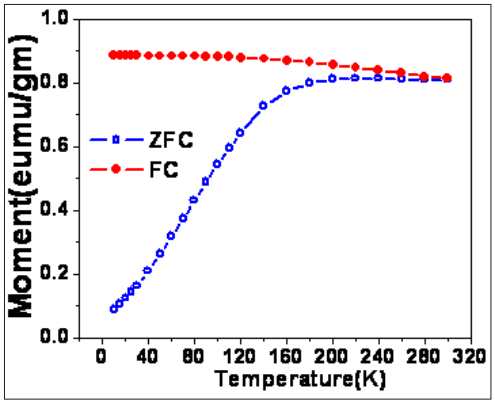

Figure 3: ZFC and FC Magnetization of BFO nanopticles as a function of temperature. Showing a sign of weak ferromagnetic behavior.

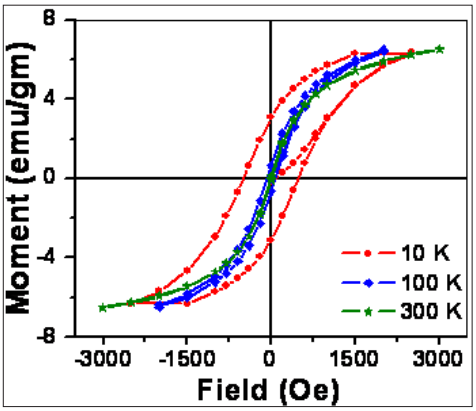

Figure 4: M-H loop for BFO at 10,100 and 300K. Distinct hysteresis is noticed.

There is a signature of magnetic phase transition below 150K, but no sign of upturn in magnetization curve characteristic of antiferromagnetic behavior observed in BFO single crystals (Purusothaman et al., 2012). Rather, in our case, there is an enhanced magnetization evident from M-T curves as well as from M-H hysteresis loops. Weak ferromagnetism in BFO often results from canting of magnetic sublattices of Fe atoms oriented antiferromagnetically and collinearly in (111) plane by the combined action of exchange interaction and spin orbit coupling (Lebeugle et al., 2007). Also, paramagnetic $Fe(3^{+})$ (probably due to presence of Fe-rich phase can account for all the low-temperature magnetic enhancement. But removing such impurities with HNO3 removes virtually all traces of ferromagnetism which has been employed in our case. Hence the enhanced magnetism is not due to Fe rich phase. There can be ferromagnetic coupling between Fe magnetic moments of two sublattices in G-type antiferromagnetic structure. Fe magnetic moments are coupled ferromagnetically within pseudocubic (111) planes. The agglomeration has brought the grains in certain fashion that a net magnetization could be derived from it. But, saturation due to complete orientation of Fe moments occurs at quite low field. However, the nanoparticle behavior is quite evident. We have also observed a sharp cusp at around 200 K in the ZFC curve around 280K. In our system of clustered nanoparticles, it is the interparticle exchange interaction that plays the dominant role in the anomalous enhancement of magnetization in the agglomerated network of particles with rhombohedrally distorted perovskite.

BFO Nanorod

There are two kinds of 1D nanostructure in the form of nanowires as well as nanorods as apparent from figs. 5a and 5b similar to earlier groups (Ederer & Spaldin, 2005; Xie et al., 2008). Fig. 5a shows the bundles of nanowires and nanorods which have come out after etching the template with NaOH. Basically they are nanorods but we observed them in the form of a bundle after etching. There is a distribution in diameters of nanorods as revealed in fig. 5a. Cross sectional view is showing development of nanorods in Fig. 5b- a representative case. It demonstrates the structures of several nanorods (around 20 in a region of 5 µm x 5 µm) with high aspect ratio protruding out of the pores after partial etching. The compositional analysis was performed by EDX analysis at different nanorods and they reflected Bi:Fe atomic ratios of slightly more than 1:1 reflecting a little more Bi content with a fluctuation within 3 per cent. Fig. 5c shows the TEM picture of nanorods of high density with intact structure. The inset indicates a clear SAED pattern with prominent rings signifying the development of polycrystalline BFO.

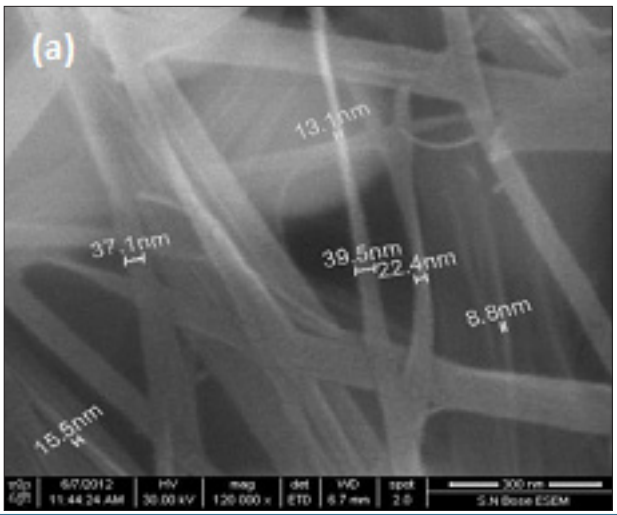

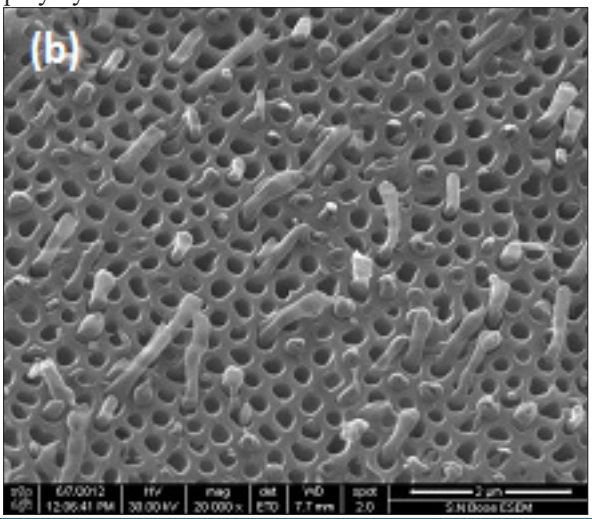

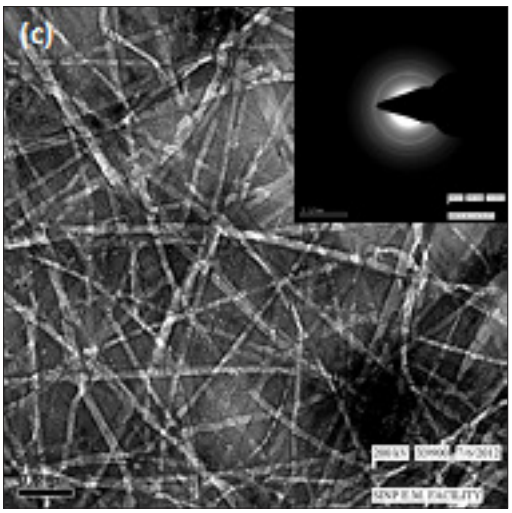

Figure 5: (a) SEM showing bundles of nanorod, (b) SEM of nanorod protruding from pores and (c) TEM of BFO nanorods and corresponding SAED pattern shown in the inset.

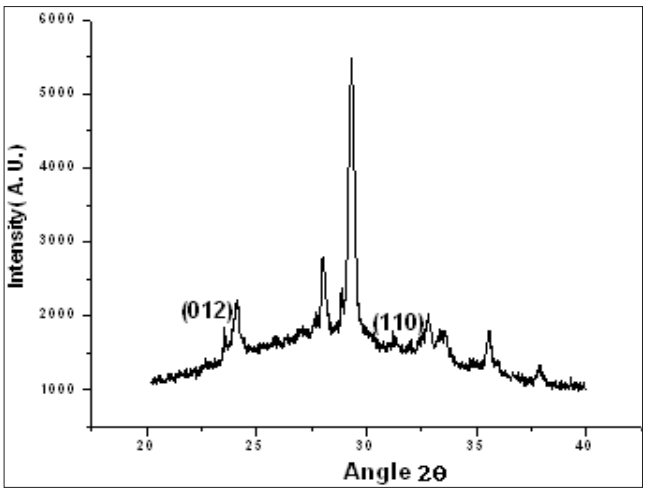

Figure 6: XRD pattern of BFO along with AAO template. Characteristic peak corresponding to 110 plane is noticed even with small amount of BFO compared to the template.

Fig.6 displays the XRD pattern of BFO nanorods along with AAO template. The dominant peaks correspond to AAO having the maximum amount. But, there is a distinct BFO characteristic peak corresponding to 110 plane. This is quite appreciable considering very small amount of BFO (around 0.5% of the wt. of the template).

Pseudocapacitance

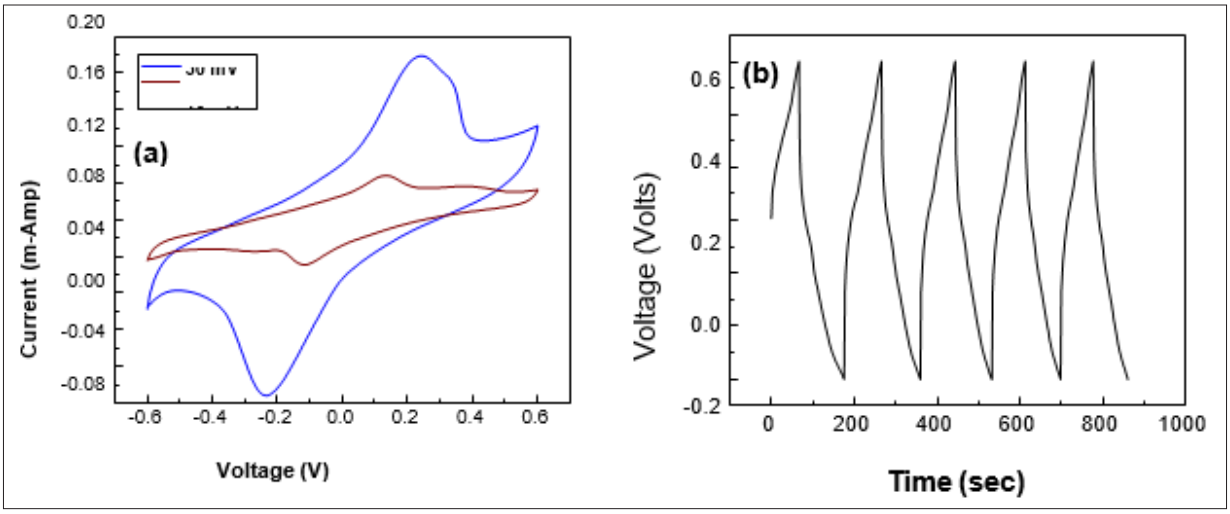

Figure 7: a. Cyclic voltammograms of samples at scanning rates of 50mV/s(blue) and 10mv/sec (red).
b. Charge discharge cycle of samples.

Typical cyclic voltammograms (CV) of different samples at a scan rate of 50 and 10mV/s between -0.6 and 0.6V in aqueous solution of 1M Na_2SO_4 are shown in Fig. 7a. Cyclic voltammograms of different samples are quite symmetrical with a mirror image of the current response from voltage, indicating ideal pseudocapacitative behavior and excellent reversibility in charging and discharging at a constant rate over the voltage range of –0.6 to 0.6V (Reddy & Reddy, 2003). Voltammetric charges (q*) at different potential scan rate *v* (mV/s) were obtained by integration of the voltammetric curves followed by division with the geometric surface area of the samples without correction for background capacitative current. The charge accumulation on BFO/AAO and AAO individually assayed by CV established that the contribution from AAO was significantly less than BFO/AAO for same weight. Typical values were 2.270×10^{-3} Coulombs for BFO/AAO and 6.45×10^{-4} Coulombs for AAO at the scanning rate of 20mv/sec.

Let us now try to understand the charge distribution in BFO/AAO template network. Our system consists of BFO nanorods some of them protruding out of pores along with porous AAO template with pore sizes varying from 20-100nm. Total charge will be distributed as inner charge in the pores (some of which contains BFO) and as outer charge on the BFO nanorods protruding 1 μm on the average above the surface of the template. Around half of the pores filled by BFO have protruded nanorods;

others are inside the pores. The depth of the pores is 60µm– the thickness of the template. Thus, the protruded portion of BFO– solely responsible for the contribution to q* is 1/60 of the wt. of protruded BFO nanorod which itself is half of the total wt. 80µgms of BFO. Rest is embedded in pores. q* (obtained by extrapolating the plot of charge q* vs. v-1/2 to v-1/2 =0 and taking the intercept) is $1.50x10^{-4}$ coulombs. On this basis, the specific capacitance of BFO nanorod structure comes out to be 450 F/gm. This large value of specific capacitance can be attributed to the nanostructure form of BFO nanorod.

The pseudocapacitative behavior of BFO stems from its redox reaction. $BiFeO_3$ is more readily reduced than oxidised, with the creation of oxygen vacancies and Fe^{2+} species. The highly unfavourable energy (> 4 eV) estimated for disproportionation of Fe3+ (to Fe^{2+} and Fe^{4+}) suggests that tetravalent iron ions are unlikely to form in this material through this process.

Conclusion

We have studied capacitance and other multiferroic properties like magnetisation of BFO nanoparticles by bottom up approach and nanorods developed on AAO templates by electrochemical means. In both cases, the presence of d electrons in the system render unique properties aided by their nanostructure. BFO nanoparicles displayed weak ferromagnetic behavior quite anomalous Capacitance of AAO as evaluated by accumulated charge is significantly less as compared to BFO. BFO nanorods protruded from the template surface demonstrated a very high specific capacitance of 450F/gm as measured from the charge accumulated on the outer surface. The high specific capacitance is due to the particular nanostructure in the form of the rod. There is a close resemblance between the capacitance assayed by CV and charge-discharge methods. The system is quite stable with respect to repeated cycling. BFO system undergoes a redox process associated with Fe(II)/Fe(III) with O vacancies being generated giving rise to pseudocapacitative behavior with high specific capacitance. The high specific capacitance in the nanorod structure coupled with stability at long cycles brings forth its application as electrodes in batteries.

Acknowledgements

Authors gratefully acknowledge Dr. P. K. Mukhopadhyay and Mr. Sakti Nath Das of S. N. Bose Center for basic Sciences for SEM studies and Mr. Pulak Kumar Roy of Saha Instititute of Nuclear Physics for TEM studies.

References

1. Zhang, X. Y., Lai, C. W., Zhao, X., Wang. D. Y., & Dai, J. Y. (2005). Synthesis and ferroelectric properties of multiferroic BiFeO3 nanotube arrays. Appl. Phys. Lett., 87, 143102-143104. DOI: https://doi.org/10.1063/1.2076437
2. Lokhande, C. D., Gujar, T. P., Shinde, U.R., Mane, R. S., & Han. S. H. (2007). Electrochemical supercapacitor application of pervoskite thin films. *Electrochem. Comm., 9*(7), 1805-1807.
DOI: https://doi.org/10.1016/j.elecom.2007.04.011
3. Gao, F., Yuan. Y., Wing, K. F., Chen, X. Y., Chen, F, Liu, J. M., & Ren, Z. F. (2006). Preparation and photoabsorption characterization of BiFeO3 nanowires. Appl. Phys. Lett., 89, 102506- 102508.
DOI: https://doi.org/10.1063/1.2345825
4. Xie, S. H., Li, J. Y., Proksch, R., Liu. Y. M., Zhou, Y. C., Liu. Y. Y., Pan. L.N., & Qiao, Y. (2008). Nanocrystalline multiferroic BiFeO3 ultrafine fibers by sol-gel based electrospinning. *Appl. Phys. Lett., 93*(22), 222904-222906. DOI: http://dx.doi.org/10.1063/1.3040010
5. Purusothaman, K. K., Cuba, M., Muralidharan, G. (2012). Supercapacitor behavior of α- MnMoO4 nanorods on different electrolytes. *Mat. Res. Bull., 47*(11), 3348–3351.
6. Lebeugle, D., Colson, D., Forget, A., Viret, M., Bonville, P., Marucco, J. F. & Fusil, S. (2007). *Phys. Rev. B, 76*(2), 024116. DOI: http://dx.doi.org/10.1103/PhysRevB.76.024116
7. Ederer, C. & Spaldin, N. A. (2005). Weak ferromagnetism and magnetoelectric coupling in bismuth ferrite. Phys. Rev. B, 71, 060401 (R).
DOI: http://dx.doi.org/10.1103/PhysRevB.71.060401
8. Reddy, R. N., & Reddy, R. G. (2003). Electrochemical Double Layer capacitance properties of carbon in aqueous and nonaqueous electrolytes. *J. Power Source,* 124, 330-33. https://studylib.net/doc/18425240/electrochemical-double-layer-capacitance-properties-of-ca...